Preprints of the 21st IFAC World Congress (Virtual)
Berlin, Germany, July 12-17, 2020

Design and Experimental Verification of Two-Dimensional Rate Limiters in Trajectory Generation for Differential Drive Robots

Anja P. R. Lauer * **Naoki Uchiyama** ** **Oliver Sawodny** ***

* *Institute for System Dynamics, University of Stuttgart, Stuttgart, Germany (e-mail: lauer@isys.uni-stuttgart.de).*
** *Department of Mechanical Engineering, Toyohashi University of Technology, Toyohashi, Japan (e-mail: uchiyama@tut.jp)*
*** *Institute for System Dynamics, University of Stuttgart, Stuttgart, Germany (e-mail: sawodny@isys.uni-stuttgart.de).*

Abstract: In order for robots to follow a desired path, velocity trajectories along the path are required. Two-dimensional rate limiters generate smooth velocity trajectories for differential drive mobile robots. First-order two-dimensional rate limiters satisfy the velocity constraints of the right and left wheel, while second-order two-dimensional rate limiters fulfill both velocity and acceleration constraints. This paper proves the global asymptotic stability of first-order two-dimensional rate limiters. It further shows the feasibility of second-order two-dimensional rate limiters by evaluating their performance through experiments with different sample paths and by comparison with a turn-on-the-spot solution.

Keywords: Trajectories, Constraints, Mobile robots, Performance evaluation

1. INTRODUCTION

Cleaning and mowing robots are becoming more and more popular, not only in private homes, but also in industrial facilities as they automate repetitive chores. In the process of cleaning or mowing, these robots have to cover a designated area. Since such robots usually carry their battery, saving energy is important both for being able to complete the task and for ecological reasons.

A coverage path planner provides a geometrical path that covers the whole area, while trajectory generation provides the time-indication for that path. A common way to generate trajectories for differential drive robots considers a motion where the robot goes straight - stops - turns on the spot because of its simplicity. Balkcom and Mason (2000), for example, derive time-optimal paths between start and goal configurations for a bounded velocity model. They prove that the fastest trajectories are composed of at most five segments. A segment is either a straight line or a rotation on the spot around the robot center.

However, unnecessary acceleration shall be avoided in this research as it is costly in terms of energy. A further requirement is that the trajectory has to satisfy the velocity and acceleration limits of the robot while the path should be followed as closely as possible. In addition, the trajectory should be generated online in order to react to dynamic obstacles. Rate limiters are a possible solution as they provide smooth trajectories while satisfying the constraints (see Sawodny et al. (2001)). This research is based on Lauer et al. (2019) who introduced multi-dimensional rate limiters for the case of differential drive mobile robots. The novelty of this paper is the stability proof of the first-order two-dimensional rate limiter and the performance evaluation of the second-order two-dimensional rate limiter through experiments. Section 2 gives the basics of the first- and second-order rate limiter. Section 3 introduces the first-order two-dimensional rate limiter and proves its stability. Section 4 extends the first-order to a second-order rate limiter. The second-order rate limiter is then tested in experiments and compared to a turn-on-the-spot solution in Section 5, followed by a conclusion in Section 6.

2. KINEMATIC MODEL AND PREREQUISITES

The kinematic model of a differential drive robot is

$$\begin{pmatrix}\dot{x}\\ \dot{y}\\ \dot{\theta}\end{pmatrix} = \begin{pmatrix}\cos\theta & 0\\ \sin\theta & 0\\ 0 & 1\end{pmatrix}\begin{pmatrix}v\\ \omega\end{pmatrix} \tag{1}$$

with position x, y and orientation θ. The linear and angular robot velocities v and ω are related to the linear velocities of the right and left wheels $v_\mathrm{R}, v_\mathrm{L}$ as

$$v = \frac{v_\mathrm{R} + v_\mathrm{L}}{2}, \qquad \omega = \frac{v_\mathrm{R} - v_\mathrm{L}}{2l}, \tag{2}$$

with the distance $2l$ between the two driven wheels. It is assumed that the robot's environment is subdivided into a grid (see Lauer et al. (2019)). A path planner provides target points that are the centers of subsequent cells, generating a piecewise linear path. The rate limiter provides a trajectory such that the robot asymptotically converges to a desired configuration. The target point is switched to the next target when a tolerance ball is reached.

3. FIRST-ORDER TWO-DIMENSIONAL RATE LIMITER

The task is to obtain reference velocities of the right and left wheels, $v_{\mathrm{R,ref}}$ and $v_{\mathrm{L,ref}}$, from the target configuration $(x_{\mathrm{S}}, y_{\mathrm{S}}, \theta_{\mathrm{S}})^{\mathrm{T}}$. First-order two-dimensional rate limiters satisfy the wheel velocity constraints

$$v_{\mathrm{R}}, v_{\mathrm{L}} \in [-v_{\mathrm{m}}, v_{\mathrm{m}}]\,. \tag{3}$$

This section explains the first-order two-dimensional rate limiter algorithm and proves its stability.

3.1 Rate limiter design

The necessary transformations have been introduced in Lauer et al. (2019). First, a desired direction vector $\boldsymbol{d}_{\mathrm{des}}$ is defined as

$$\boldsymbol{d}_{\mathrm{des}} = \begin{pmatrix} \cos\theta_{\mathrm{loc}} & \sin\theta_{\mathrm{loc}} \\ -\sin\theta_{\mathrm{loc}} & \cos\theta_{\mathrm{loc}} \end{pmatrix} \begin{pmatrix} x_{\mathrm{S}} - x_{\mathrm{loc}} \\ y_{\mathrm{S}} - y_{\mathrm{loc}} \end{pmatrix} = \begin{pmatrix} d_{\mathrm{des},x} \\ d_{\mathrm{des},y} \end{pmatrix}, \tag{4}$$

with the current configuration $(x_{\mathrm{loc}}, y_{\mathrm{loc}}, \theta_{\mathrm{loc}})^{\mathrm{T}}$. This desired direction vector often requires the robot to instantaneously change its orientation. Because of the kinematic constraints, the robot usually cannot execute this movement. Thus, desired values for the linear and angular robot velocity $(v_{\mathrm{des}}, \omega_{\mathrm{des}})$ are found to approximate $\boldsymbol{d}_{\mathrm{des}}$. For the mapping $\boldsymbol{d}_{\mathrm{des}} \mapsto (v_{\mathrm{des}}, \omega_{\mathrm{des}})$, $\boldsymbol{d}_{\mathrm{des}}$ is transformed to polar coordinates (see Fig. 1)

$$\begin{aligned} r\left(\boldsymbol{d}_{\mathrm{des}}\right) &= \sqrt{\left(d_{\mathrm{des},x}\right)^2 + \left(d_{\mathrm{des},y}\right)^2}, \\ \varphi\left(\boldsymbol{d}_{\mathrm{des}}\right) &= \operatorname{atan2}\left(d_{\mathrm{des},y}, d_{\mathrm{des},x}\right), \end{aligned} \tag{5}$$

where $r\left(\boldsymbol{d}_{\mathrm{des}}\right)$ is the length of $\boldsymbol{d}_{\mathrm{des}}$ and $\varphi\left(\boldsymbol{d}_{\mathrm{des}}\right)$ is the current orientation error. The polar coordinates are amplified with the tunable gains k_1 and k_2 to the desired velocities

$$\begin{aligned} v_{\mathrm{des}} &= k_1 r\left(\boldsymbol{d}_{\mathrm{des}}\right) \cos\left(\varphi\left(\boldsymbol{d}_{\mathrm{des}}\right)\right), \\ \omega_{\mathrm{des}} &= k_2 \varphi\left(\boldsymbol{d}_{\mathrm{des}}\right). \end{aligned} \tag{6}$$

The cosine term in (6) reduces the robot velocity when the orientation of the robot is largely off. This avoids overshooting behavior.

The obtained desired velocities $(v_{\mathrm{des}}, \omega_{\mathrm{des}})$ do not necessarily fulfill the constraints on (v, ω)

$$\underbrace{\begin{pmatrix} 1 & l \\ -1 & -l \\ 1 & -l \\ -1 & l \end{pmatrix}}_{\boldsymbol{A}_{\mathrm{ineq}}} \begin{pmatrix} v \\ \omega \end{pmatrix} \leq \underbrace{\begin{pmatrix} v_{\mathrm{m}} \\ v_{\mathrm{m}} \\ v_{\mathrm{m}} \\ v_{\mathrm{m}} \end{pmatrix}}_{\boldsymbol{v}_{\mathrm{m}}}, \tag{7}$$

and can lie outside of the bounded convex constraint set

$$K_1 = \left\{ v, \omega \,\middle|\, \boldsymbol{A}_{\mathrm{ineq}} \begin{pmatrix} v \\ \omega \end{pmatrix} \leq \boldsymbol{v}_{\mathrm{m}} \right\} \tag{8}$$

which is illustrated in Fig. 2. Taking the maximum linear velocity v_{m} and the maximum angular velocity v_{m}/l at the same time results in Z_1 which lies outside of the feasible set. Such tuples $(v_{\mathrm{des}}, \omega_{\mathrm{des}})$ are mapped to feasible reference velocities $(v_{\mathrm{ref}}, \omega_{\mathrm{ref}})$. This second mapping $(v_{\mathrm{des}}, \omega_{\mathrm{des}}) \mapsto (v_{\mathrm{ref}}, \omega_{\mathrm{ref}})$ is inspired by the Kalai-Smorodinsky bargaining solution (see Kalai and Smorodinsky (1975)) and implements a solution as follows:

$$\begin{aligned} v_{\mathrm{ref}} &= \begin{cases} v_{\mathrm{des}} & \text{if } (v_{\mathrm{des}}, \omega_{\mathrm{des}}) \in K_1 \\ v_{\mathrm{m}} \frac{v_{\mathrm{des}}}{|v_{\mathrm{des}}| + |l\omega_{\mathrm{des}}|} & \text{otherwise,} \end{cases} \\ \omega_{\mathrm{ref}} &= \begin{cases} \omega_{\mathrm{des}} & \text{if } (v_{\mathrm{des}}, \omega_{\mathrm{des}}) \in K_1 \\ v_{\mathrm{m}} \frac{\omega_{\mathrm{des}}}{|v_{\mathrm{des}}| + |l\omega_{\mathrm{des}}|} & \text{otherwise.} \end{cases} \end{aligned} \tag{9}$$

Equation (9) maps the infeasible desired velocity tuple to exactly the one boundary point of the feasible set which lies on a straight line between the desired point and the origin, yielding both a short running time and a solution with a fair tradeoff between linear and angular velocities. The reference velocities $(v_{\mathrm{des}}, \omega_{\mathrm{des}})$ are transformed to the wheel velocities using (2). The structure of the first-order two-dimensional rate limiter is shown in Fig. 3.

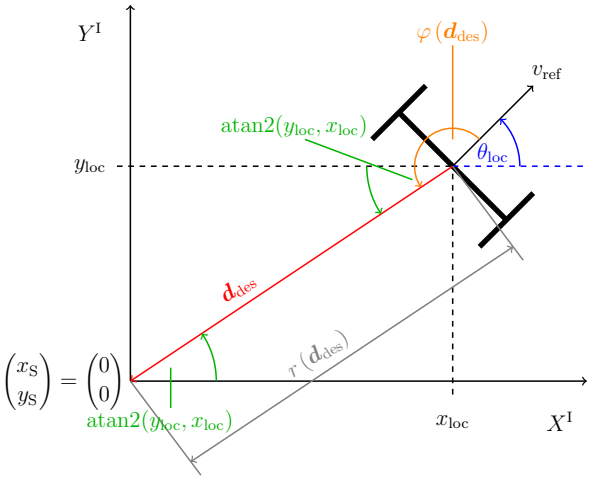

Fig. 1. Polar coordinates and desired direction vector.

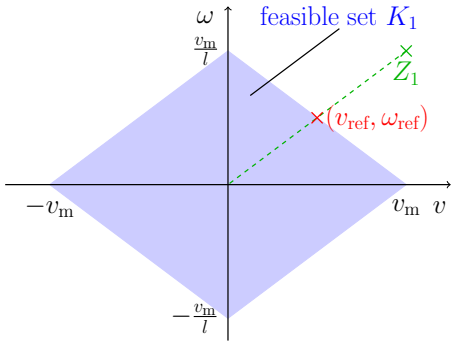

Fig. 2. Set of feasible v and ω.

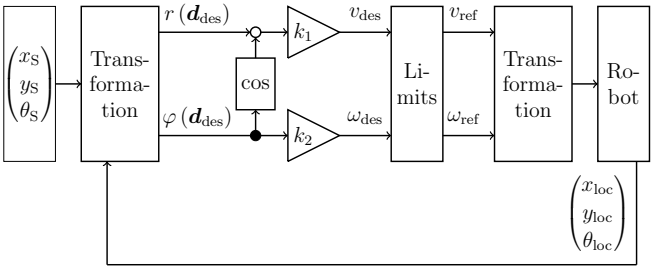

Fig. 3. Block diagram of the first-order two-dimensional rate limiter.

3.2 Stability analysis

The stability of the first-order two-dimensional rate limiter is analyzed using Artstein's Theorem (see Sontag (1989)) as follows:

Theorem 1. **Artstein's Theorem**: A Control Lyapunov Function (CLF) exists if and only if there is an $f : \mathbb{R}^n \to \mathbb{R}^m$ s.t. the equilibrium $x^* = 0$ becomes globally asymptotically stable under $u(t) = f(x(t))$.

Theorem 2. **Stability of first-order two-dimensional rate limiters**: First-order two-dimensional rate limiters are globally asymptotically stable for $v_{\mathrm{ref}} = k_1 r\cos\varphi$, $\omega_{\mathrm{ref}} = k_2\varphi$ in the case $k_1 = \frac{1}{2}k_2 = k > 0$.

Proof. Considering the kinematic model

$$\begin{aligned}\dot{x}_{\mathrm{loc}} &= v_{\mathrm{ref}}\cos\theta_{\mathrm{loc}},\\ \dot{y}_{\mathrm{loc}} &= v_{\mathrm{ref}}\sin\theta_{\mathrm{loc}},\\ \dot{\theta}_{\mathrm{loc}} &= \omega_{\mathrm{ref}},\end{aligned} \tag{10}$$

the aim is to stabilize the position $(x_{\mathrm{loc}}, y_{\mathrm{loc}}) = (0,0)$ as time goes to infinity. The desired direction vector is

$$\begin{aligned}\boldsymbol{d}_{\mathrm{des}} &= \begin{pmatrix}\cos\theta_{\mathrm{loc}}\,(0-x_{\mathrm{loc}}) + \sin\theta_{\mathrm{loc}}\,(0-y_{\mathrm{loc}})\\ -\sin\theta_{\mathrm{loc}}\,(0-x_{\mathrm{loc}}) + \cos\theta_{\mathrm{loc}}\,(0-y_{\mathrm{loc}})\end{pmatrix}\\ &= \left(d_{\mathrm{des,x}}, d_{\mathrm{des,y}}\right)^{\mathrm{T}}.\end{aligned} \tag{11}$$

The system is transformed to polar coordinates (r,φ,θ) where

$$\theta = \theta_{\mathrm{loc}} \text{ and} \tag{12}$$

$$r = r\left(\boldsymbol{d}_{\mathrm{des}}\right) = \sqrt{d_{\mathrm{des,x}}^2 + d_{\mathrm{des,y}}^2} = \sqrt{x_{\mathrm{loc}}^2 + y_{\mathrm{loc}}^2}. \tag{13}$$

From Fig. 1, the orientation for the robot to be headed towards the origin is

$$\varphi = \varphi\left(\boldsymbol{d}_{\mathrm{des}}\right) = \operatorname{atan2}(y_{\mathrm{loc}}, x_{\mathrm{loc}}) + \pi - \theta \tag{14}$$

and the current position $(x_{\mathrm{loc}}, y_{\mathrm{loc}})$ is

$$\begin{aligned}x_{\mathrm{loc}} &= r\cos(\operatorname{atan2}(y_{\mathrm{loc}}, x_{\mathrm{loc}})) = -r\cos(\varphi+\theta),\\ y_{\mathrm{loc}} &= r\sin(\operatorname{atan2}(y_{\mathrm{loc}}, x_{\mathrm{loc}})) = -r\sin(\varphi+\theta).\end{aligned} \tag{15}$$

The robot dynamics in the coordinates (r,φ,θ) are

$$\begin{aligned}\dot{\theta} &= \omega_{\mathrm{ref}},\\ \dot{r} &= \frac{\mathrm{d}}{\mathrm{d}t}\left(\sqrt{x_{\mathrm{loc}}^2 + y_{\mathrm{loc}}^2}\right) = \frac{x_{\mathrm{loc}}\dot{x}_{\mathrm{loc}} + y_{\mathrm{loc}}\dot{y}_{\mathrm{loc}}}{\sqrt{x_{\mathrm{loc}}^2 + y_{\mathrm{loc}}^2}}\\ &= \frac{1}{r}\left(-r\cos(\varphi+\theta)\,v_{\mathrm{ref}}\cos\theta - r\sin(\varphi+\theta)\,v_{\mathrm{ref}}\sin\theta\right)\\ &= -v_{\mathrm{ref}}\cos\varphi,\\ \dot{\varphi} &= \frac{\mathrm{d}}{\mathrm{d}t}\left(\operatorname{atan2}(y_{\mathrm{loc}}, x_{\mathrm{loc}}) + \pi - \theta\right)\\ &= -\omega_{\mathrm{ref}} + \frac{1}{1+\left(\frac{y_{\mathrm{loc}}}{x_{\mathrm{loc}}}\right)^2}\frac{\mathrm{d}}{\mathrm{d}t}\left(\frac{y_{\mathrm{loc}}}{x_{\mathrm{loc}}}\right)\\ &= -\omega_{\mathrm{ref}} + \frac{v_{\mathrm{ref}}}{r}\sin\varphi.\end{aligned} \tag{16}$$

From Artstein's Theorem (see Theorem 1), if a CLF (see Freeman and Kokotović (2008)) can be found, there exists a stabilizing input. For this system in the coordinates (r,φ,θ), the CLF candidate V_1 is defined by

$$V_1 = r^2(2-\cos\varphi). \tag{17}$$

This candidate is a CLF if the Lie derivative can be made negative definite. This Lie derivative is

$$\begin{aligned}\dot{V}_1 &= 2r\dot{r}(2-\cos\varphi) + r^2(\sin\varphi)\dot{\varphi}\\ &= \left(-2r(2-\cos\varphi)\cos\varphi + r\sin^2\varphi\right)v_{\mathrm{ref}} - r^2(\sin\varphi)\omega_{\mathrm{ref}}.\end{aligned} \tag{18}$$

Choosing $(v_{\mathrm{ref}}, \omega_{\mathrm{ref}})$ as

$$\begin{aligned}v_{\mathrm{ref}} &= k_1 r\cos\varphi = v_{\mathrm{des}},\\ \omega_{\mathrm{ref}} &= k_2\varphi = \omega_{\mathrm{des}},\end{aligned} \tag{19}$$

renders the Lie derivative negative definite:

$$\begin{aligned}\dot{V}_1 &= -2k_1V_1\cos^2\varphi + k_1r^2\left(\sin^2\varphi\right)\cos\varphi - k_2r^2\varphi\sin\varphi\\ &\overset{(\star)}{\leq} -2k_1V_1\cos^2\varphi + k_1r^2\left(\sin^2\varphi\right)\cos\varphi - k_2r^2\sin^2\varphi\\ &= -2k_1V_1\cos^2\varphi - k_1\left(\sin^2\varphi\right)r^2\left(\frac{k_2}{k_1} - \cos\varphi\right).\end{aligned} \tag{20}$$

In $(\star)$ the fact that $\varphi\sin\varphi \geq \sin^2\varphi$ for $\varphi \in [-\pi,\pi]$ was used. It can be assumed that φ is projected into this interval. For $k_1 = \frac{1}{2}k_2 = k > 0$,

$$\begin{aligned}\dot{V}_1 &\leq -2kV_1\cos^2\varphi - kV_1\sin^2\varphi\\ &= -kV_1 - kV_1\cos^2\varphi\\ &\leq -kV_1\\ &< 0.\end{aligned} \tag{21}$$

Thus, according to Artstein's Theorem, the inputs $v_{\mathrm{ref}} = k_1 r\cos\varphi$, $\omega_{\mathrm{ref}} = k_2\varphi$ stabilize the system. The Lie derivative of V_1 in (18) depends linearly on the control vector $\boldsymbol{u}_1 = (v_{\mathrm{ref}}, \omega_{\mathrm{ref}})^{\mathrm{T}}$. Therefore, also $\boldsymbol{u}_1 = \hat{k}\cdot(v_{\mathrm{ref}}, \omega_{\mathrm{ref}})^{\mathrm{T}}$ with $\hat{k} > 0$ yields a negative definite Lie derivative $\dot{V}_1 \leq -\hat{k}kV_1$. So, the desired values $v_{\mathrm{des}} = k_1 r\cos\varphi$ and $\omega_{\mathrm{des}} = k_2\varphi$ in (6) are a suitable choice. The parameters k_1 and k_2 yield an additional freedom to optimize the performance of the trajectory generation.

Following the argumentation that $\hat{k}\cdot(v_{\mathrm{ref}}, \omega_{\mathrm{ref}})^{\mathrm{T}}$ renders $\dot{V}_1$ negative definite, also the concatenation of $\boldsymbol{u}_1$ with the rate limiter, which multiplies a positive real number $\hat{k} = v_{\mathrm{m}}/\left(|v_{\mathrm{des}}| + |l\omega_{\mathrm{des}}|\right)$, renders the Lie derivative negative definite. With the mapping policy (9), we can summarize

$$\dot{V}_1 \leq \begin{cases} -kV_1 & \text{if } (v_{\mathrm{des}}, \omega_{\mathrm{des}}) \in K_1\\ -\frac{v_{\mathrm{m}}}{|v_{\mathrm{des}}|+|l\omega_{\mathrm{des}}|}kV_1 & \text{otherwise.}\end{cases} \tag{22}$$

□

Based on these considerations, the first-order rate limiter is extended to a second-order rate limiter, which can limit both velocities and accelerations.

4. SECOND-ORDER TWO-DIMENSIONAL RATE LIMITER

The second-order two-dimensional rate limiter satisfies the wheel velocity and acceleration constraints

$$v_{\mathrm{R}}, v_{\mathrm{L}} \in [-v_{\mathrm{m}}, v_{\mathrm{m}}], \qquad \dot{v}_{\mathrm{R}}, \dot{v}_{\mathrm{L}} \in [-\dot{v}_{\mathrm{m}}, \dot{v}_{\mathrm{m}}]. \tag{23}$$

Therefore, the first-order two-dimensional rate limiter is extended as follows: The braking distances

$$x_{\mathrm{B}} = \frac{\dot{x}_{\mathrm{ref}}\cdot|\dot{x}_{\mathrm{ref}}|}{2\dot{v}_{\mathrm{m}}}, \qquad y_{\mathrm{B}} = \frac{\dot{y}_{\mathrm{ref}}\cdot|\dot{y}_{\mathrm{ref}}|}{2\dot{v}_{\mathrm{m}}} \tag{24}$$

with the current reference velocities $\dot{x}_{\mathrm{ref}}$, $\dot{y}_{\mathrm{ref}}$ and the current linear robot reference velocity v_{ref},

$$\begin{aligned}\dot{x}_{\mathrm{ref}} &= v_{\mathrm{ref}}\cos\theta_{\mathrm{loc}},\\ \dot{y}_{\mathrm{ref}} &= v_{\mathrm{ref}}\sin\theta_{\mathrm{loc}},\end{aligned} \tag{25}$$

are considered to avoid overshooting of the position. With the correction terms

$$\begin{aligned} x_{\mathrm{E}} &= x_{\mathrm{B}} + x_{\mathrm{loc}}, \\ y_{\mathrm{E}} &= y_{\mathrm{B}} + y_{\mathrm{loc}}, \end{aligned} \tag{26}$$

the desired direction vector $\boldsymbol{d}_{\mathrm{des}}$ is

$$\boldsymbol{d}_{\mathrm{des}} = \begin{pmatrix} \cos\theta_{\mathrm{loc}} & \sin\theta_{\mathrm{loc}} \\ -\sin\theta_{\mathrm{loc}} & \cos\theta_{\mathrm{loc}} \end{pmatrix} \begin{pmatrix} x_{\mathrm{S}} - x_{\mathrm{E}} \\ y_{\mathrm{S}} - y_{\mathrm{E}} \end{pmatrix}. \tag{27}$$

This is transformed into polar coordinates and amplified to desired velocities $(v_{\mathrm{des}}, \omega_{\mathrm{des}})$ as in the approach in Section 3. The Kalai–Smorodinsky bargaining solution (see Kalai and Smorodinsky (1975)) inspires $(v_{\mathrm{des}}, \omega_{\mathrm{des}}) \mapsto (v_{\mathrm{S}}, \omega_{\mathrm{S}})$:

$$\begin{aligned} v_{\mathrm{S}} &= \begin{cases} v_{\mathrm{des}} & \text{if } (v_{\mathrm{des}}, \omega_{\mathrm{des}}) \in K_1 \\ v_{\mathrm{m}} \frac{v_{\mathrm{des}}}{|v_{\mathrm{des}}| + |l\omega_{\mathrm{des}}|} & \text{otherwise,} \end{cases} \\ \omega_{\mathrm{S}} &= \begin{cases} \omega_{\mathrm{des}} & \text{if } (v_{\mathrm{des}}, \omega_{\mathrm{des}}) \in K_1 \\ v_{\mathrm{m}} \frac{\omega_{\mathrm{des}}}{|v_{\mathrm{des}}| + |l\omega_{\mathrm{des}}|} & \text{otherwise.} \end{cases} \end{aligned} \tag{28}$$

The input of the acceleration limitation block is obtained by amplifying

$$\begin{aligned} v_{\mathrm{A}} &= v_{\mathrm{S}} - v_{\mathrm{ref}}, \\ \omega_{\mathrm{A}} &= \omega_{\mathrm{S}} - \omega_{\mathrm{ref}}, \end{aligned} \tag{29}$$

with the tunable gains k_3 and k_4 to

$$\begin{aligned} \dot{v}_{\mathrm{A}} &= k_3 v_{\mathrm{A}}, \\ \dot{\omega}_{\mathrm{A}} &= k_4 \omega_{\mathrm{A}}. \end{aligned} \tag{30}$$

Then, another coupled limitation block ensures that the acceleration constraints are fulfilled analogously to the velocity constraints:

$$\begin{aligned} \dot{v}_{\mathrm{ref}} &= \begin{cases} \dot{v}_{\mathrm{A}} & \text{if } (\dot{v}_{\mathrm{A}}, \dot{\omega}_{\mathrm{A}}) \in K_2 \\ \dot{v}_{\mathrm{m}} \frac{\dot{v}_{\mathrm{A}}}{|\dot{v}_{\mathrm{A}}| + |l\dot{\omega}_{\mathrm{A}}|} & \text{otherwise,} \end{cases} \\ \dot{\omega}_{\mathrm{ref}} &= \begin{cases} \dot{\omega}_{\mathrm{A}} & \text{if } (\dot{v}_{\mathrm{A}}, \dot{\omega}_{\mathrm{A}}) \in K_2 \\ \dot{v}_{\mathrm{m}} \frac{\dot{\omega}_{\mathrm{A}}}{|\dot{v}_{\mathrm{A}}| + |l\dot{\omega}_{\mathrm{A}}|} & \text{otherwise.} \end{cases} \end{aligned} \tag{31}$$

The feasible set K_2 is, analogously to (8),

$$K_2 = \left\{ \dot{v}, \dot{\omega} \middle| A_{\mathrm{ineq}} \begin{pmatrix} \dot{v} \\ \dot{\omega} \end{pmatrix} \leq \dot{\boldsymbol{v}}_{\mathrm{m}} \right\}. \tag{32}$$

The reference robot accelerations from (31) are integrated and then transformed to the reference wheel velocities.

5. EXPERIMENTS

In this section, the experimental setup is described. Then, a turn-on-the-spot solution is tested on a rectangular path and compared to the rate limiter performance.

5.1 Experimental setup

The trajectory generation with the described second-order two-dimensional rate limiter was tested with the following setup. The algorithm is implemented in MATLAB. In the ROS network, the MATLAB node communicates with the ROS-master via Wifi. The experimental robot is controlled by the on-board ROS-master PC, which can set the current reference velocities $v_{\mathrm{R,ref}}$ and $v_{\mathrm{L,ref}}$. A proprietary black-box kinematic controller generates the current inputs for the motors from the reference velocities. The feedforward trajectory generation algorithm in MATLAB sends the reference velocities to the ROS-master via publishers with sampling time $t_{\mathrm{samp}} = 100\,\mathrm{ms}$, which shows the real-time capability of the algorithm. Any localization algorithm, sensor feedback and position controller were not used in the experiment. The wheel velocities were measured by wheel encoders and integrated to positions. The MATLAB node reads the sensor data via subscribers. Several disturbances affect this experiment:

- The communication between MATLAB and ROS via Wifi depends on the signal strength and causes time delays. Not all time steps are exactly 100 ms.
- The wheel encoder measurements include noise.
- The robot has a proprietary black-box kinematic controller which cannot be accessed nor changed.

The rate limiter was tested with the maximum rates $v_{\mathrm{m}} = 0.3\,\mathrm{m/s}$ and $\dot{v}_{\mathrm{m}} = 0.5\,\mathrm{m/s^2}$ and the gains $k_1 = 4\,\mathrm{1/s}$, $k_2 = 10\,\mathrm{1/s}$, $k_3 = 10\,\mathrm{1/s}$, $k_4 = 10\,\mathrm{1/s}$ on four different sample paths (see Table 1). In the following, "wide curve" means that, due to a higher error tolerance, the curve radius is greater than the radius of a "narrow curve". The performance of the rate limiter solution is compared to the performance of a turn-on-the-spot solution, which makes the robot go straight - stop - turn on the spot, for a $2\,\mathrm{m} \times 1\,\mathrm{m}$ rectangular path. Fig. 4 shows that the simulated and measured paths from the second-order two-dimensional rate limiter are smooth. The measured paths deviate from the simulated paths due to the disturbances mentioned above.

Table 1. Experimental conditions.

Sample path	Error tolerance in [m]	Cell size in [m]	Path length in [m]
Rectangle wide curves	0.3	0.8	6
Rectangle narrow curves	0.0757	0.3	6
Path 3	0.0757	0.3	6.45
Path 4	0.0757	0.3	7.2

5.2 Turn-on-the-spot solution on a rectangular path

The turn-on-the-spot solution is generated using third-order polynomials for the velocity with the initial and end conditions $\ddot{x} = 0$, $\dot{x} = \dot{x}_{\mathrm{S}}$, $x = x_{\mathrm{S}}$. Only velocity limits are considered. Fig. 5 shows the reference and measured velocities of the right wheel, while Fig. 6 is for the left wheel. The linear robot velocity in Fig. 7 shows that the robot does not move smoothly, but stops in order to turn.

5.3 Rate limiter on a rectangular path with wide curves

The rate limiter generates a motion on a higher velocity level than the turn-on-the-spot solution and makes the robot not stop at corners, but continue forward as in Fig. 7. Therefore, the turn-on-the-spot solution is slower with 31.8 s to complete the course, while the smooth second-order two-dimensional rate limiter is faster with 22.3 s in the case of wide curves. The simulated and measured wheel accelerations and velocities of the rectangular path with wide curves are shown in Figs. 8 - 11. The measured accelerations in Figs. 8 and 9 were low-pass filtered. In the simulations, the constraints are satisfied. In the experiments, the disturbances mentioned above distort the results.

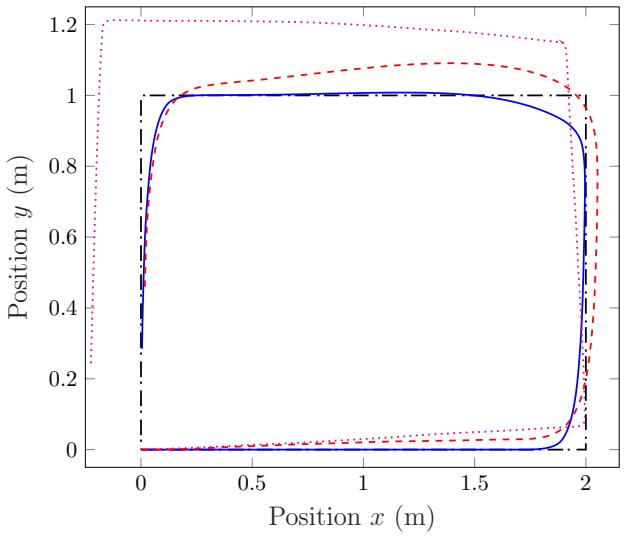

Fig. 4. Simulated and measured paths comparing the rate limiter and the turn-on-the-spot solution for a wide-curved rectangular path. -·-·-: Desired path. —: Simulated path (rate limiter). – –: Measured path (rate limiter). ····: Measured path (turn-on-the-spot).

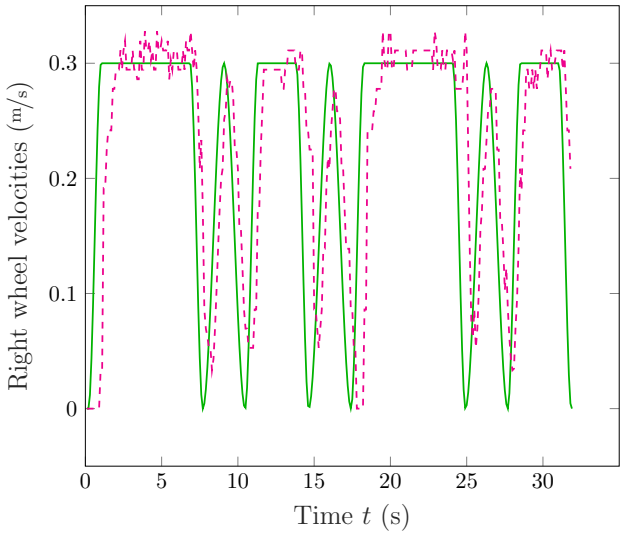

Fig. 5. Right wheel velocities for a wide-curved rectangular path and the turn-on-the-spot solution. —: Reference $v_{\mathrm{R,ref}}$. – –: Measured $v_{\mathrm{R,enc}}$.

5.4 Evaluation

The low RMSE values in Table 2 show that the measured velocities can follow the reference velocities. Furthermore, the experiments show the real-time capability of the proposed algorithm. In addition, the generated smooth path may provide an energy-saving effect compared to the turn-on-the-spot solution as unnecessary acceleration due to stopping is avoided.

6. CONCLUSION AND FUTURE WORK

This paper continued the work in Lauer et al. (2019) by showing the global asymptotic stability of the first-order two-dimensional rate limiter. The simulation studies

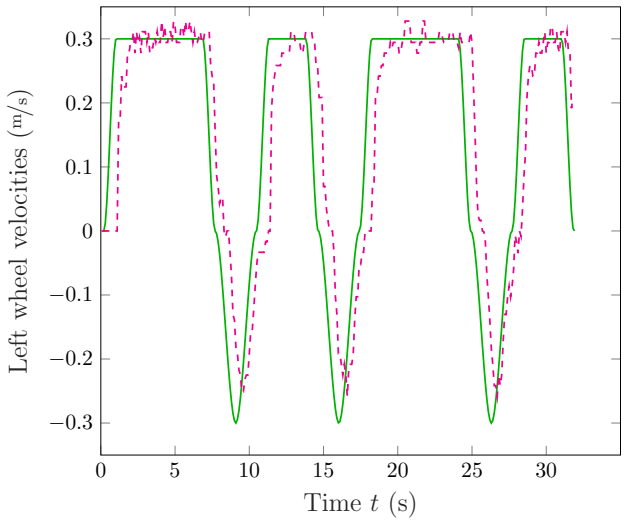

Fig. 6. Left wheel velocities for a wide-curved rectangular path and the turn-on-the-spot solution. —: Reference $v_{\mathrm{L,ref}}$. – –: Measured $v_{\mathrm{L,enc}}$.

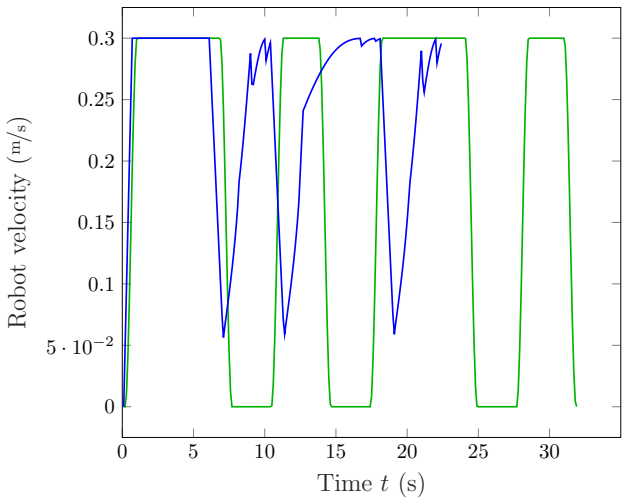

Fig. 7. Comparison of the reference linear robot velocity between the turn-on-the-spot solution and the rate limiter for a wide-curved rectangular path. —: Turn-on-the-spot. —: Rate limiter.

and experiments, which were conducted for several sample paths, show that the second-order two-dimensional rate limiter trajectory generation is feasible as the results achieve good path following. The rate limiter generates smooth paths and has thus a shorter running time than the turn-on-the-spot solution. The experiments further show the real-time capability of the algorithm. The short computation time yields the possibility to generate trajectories online and to incorporate dynamic obstacles by inserting

Table 2. RMSE of the experiments in [m/s].

Sample path	Robot velocity	Right wheel velocity	Left wheel velocity
Rectangle wide curves	0.0616	0.0382	0.1049
Rectangle narrow curves	0.0863	0.0705	0.1639
Path 3	0.1092	0.1549	0.2292
Path 4	0.1264	0.2762	0.1077

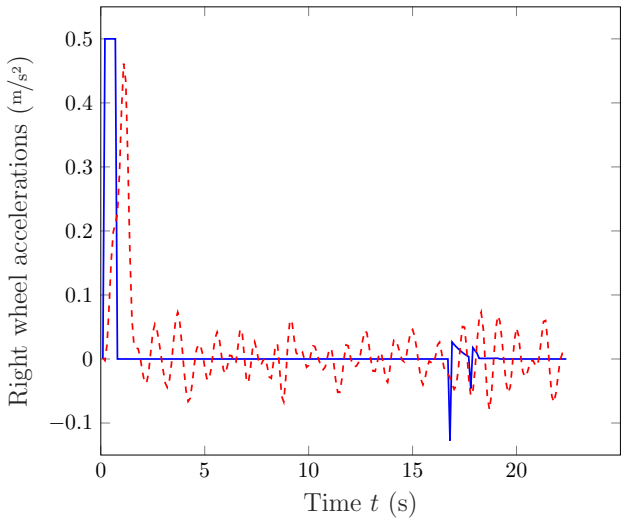

Fig. 8. Right wheel accelerations for a wide-curved rectangular path and the rate limiter. —: Reference $\dot{v}_{\mathrm{R,ref}}$. – –: Measured $\dot{v}_{\mathrm{R,enc}}$.

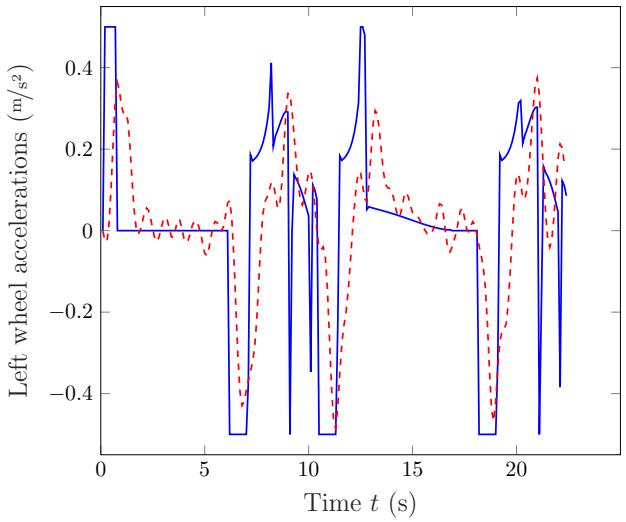

Fig. 9. Left wheel accelerations for a wide-curved rectangular path and the rate limiter. —: Reference $\dot{v}_{\mathrm{L,ref}}$. – –: Measured $\dot{v}_{\mathrm{L,enc}}$.

new waypoints. Moreover, the rate limiter is expected to save energy compared to the turn-on-the-spot solution as it avoids stopping and accelerating.

The stability of two-dimensional rate limiters for higher orders will be left for future work. A localization algorithm and a position controller to improve the performance and increase the safety of the system will also be considered. Furthermore, the algorithm can be implemented in ROS directly to avoid the communication via Wifi.

REFERENCES

Balkcom, D.J. and Mason, M.T. (2000). Time optimal trajectories for bounded velocity differential drive robots. *IEEE International Conference on Robotics and Automation*, 3, 2499–2504.

Freeman, R.A. and Kokotović, P.V. (2008). *Robust nonlinear control design: State-space and Lyapunov techniques.*

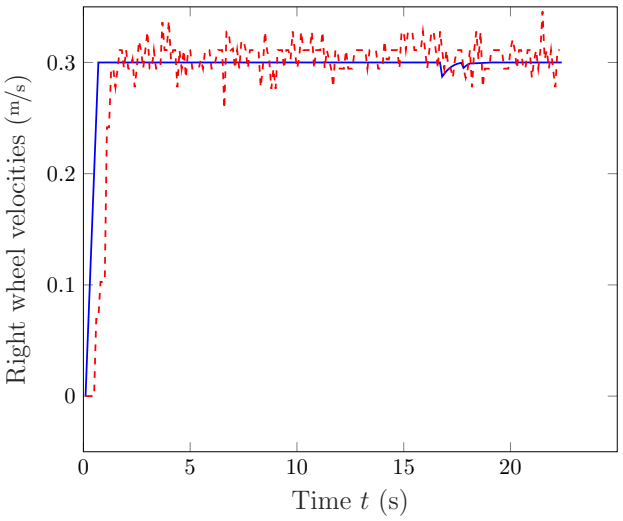

Fig. 10. Right wheel velocities for a wide-curved rectangular path and the rate limiter. —: Reference $v_{\mathrm{R,ref}}$. – –: Measured $v_{\mathrm{R,enc}}$.

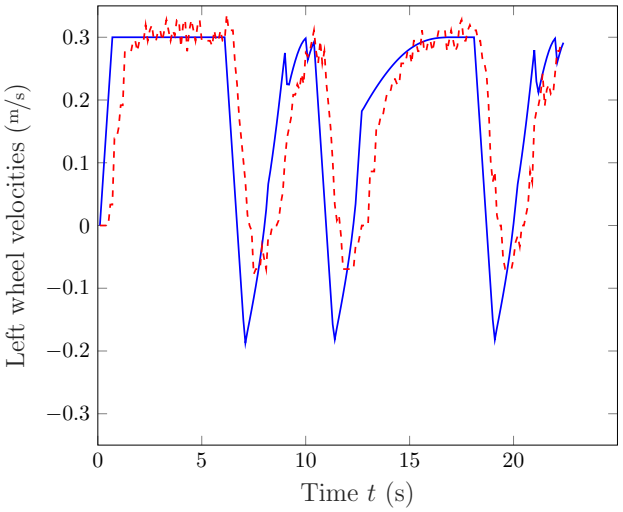

Fig. 11. Left wheel velocities for a wide-curved rectangular path and the rate limiter. —: Reference $v_{\mathrm{L,ref}}$. – –: Measured $v_{\mathrm{L,enc}}$.

Modern Birkhäuser classics. Birkhäuser, Boston, Mass., reprint of the 1996 ed. edition.

Kalai, E. and Smorodinsky, M. (1975). Other solutions to Nash's bargaining problem. *Econometrica*, 43(3).

Lauer, A.P.R., Uchiyama, N., and Sawodny, O. (2019). Online trajectory generation for differential drive mobile robots using multi-dimensional rate limiters. In *2019 International Electronics Symposium (IES)*, 31–36. IEEE.

Sawodny, O., Aschemann, H., and Bulach, A. (2001). Online generation of trajectories considering kinematic constraints. *Proceedings of 7th IEEE Int. Conference on Methods & Models in Automation & Robotics.*

Sontag, E.D. (1989). A 'universal' construction of Artstein's theorem on nonlinear stabilization. *Systems & Control Letters*, 13(2), 117–123.